# Influence of the Initial Morphology on the Elasticity of Oriented Syndiotactic Polypropylene

**ARTICLE** *in* MACROMOLECULES · JULY 2004

Impact Factor: 5.8 · DOI: 10.1021/ma040039e



**3 AUTHORS:**

Liberata Guadagno
Università degli Studi di Salerno
**112** PUBLICATIONS **1,254** CITATIONS
SEE PROFILE

Concetta D'Aniello
Università degli Studi di Salerno
**30** PUBLICATIONS **478** CITATIONS
SEE PROFILE

Carlo Naddeo
Università degli Studi di Salerno
**53** PUBLICATIONS **656** CITATIONS
SEE PROFILE

# Influence of the Initial Morphology on the Elasticity of Oriented Syndiotactic Polypropylene

**Liberata Guadagno, Concetta D'Aniello, Carlo Naddeo, and Vittoria Vittoria***

*Dipartimento di Ingegneria Chimica e Alimentare, Università di Salerno, Via Ponte Don Melillo, 1-84084 Fisciano (Salerno), Italy*

**Stefano Valdo Meille**

*Dipartimento di Chimica, Materiali ed Ingegneria Chimica "G. Natta", Politecnico di Milano, Via Mancinelli, 7-20131 Milano, Italy*

*Received February 18, 2004; Revised Manuscript Received May 12, 2004*

ABSTRACT: The influence of the initial phase composition and crystallite size on the mechanical properties and the elastic behavior of oriented syndiotactic polypropylene (sPP) was investigated. Two samples ($A_{25}$ and $B_{100}$) were crystallized from the melt respectively at 25 and 100 °C, obtaining the same crystalline forms but different morphologies, in terms of crystallinity, crystal dimensions, and phase composition. X-ray diffraction was used to determine the crystallinity and the crystal dimensions, whereas the vapor transport properties allowed to evidence and quantify the presence of an intermediate phase. Sample $A_{25}$ shows smaller crystals, lower crystallinity, and a lower amorphous fraction but a larger mesomorphic component as compared to $B_{100}$. The two samples were then stretched to a draw ratio of 7. They showed very different stress−strain curves, which appear to correlate with the initial structure. On releasing the tension both fibers undergo a large shrinkage, reaching $\lambda = 4$. The presence of the trans-planar form III and of the trans-planar mesophase characterize the fiber $A_{25}$ at $\lambda = 7$ while upon relaxation only the trans-planar mesophase and a small fraction of an oriented helical polymorph are apparent. In the fully extended fiber $B_{100}$ well-oriented form III and small amounts of a modestly oriented helical form were evidenced. The relaxed fiber $B_{100}$ contains an essentially unchanged crystalline helical component along with the trans-planar mesophase. Stress−strain cycles of fibers $A_{25}$ and $B_{100}$ allowed the determination of the hysteresis curves and the permanent set. The stress−strain data were evaluated in terms of the Mooney−Rivlin equation and show for fiber $B_{100}$, with a more substantial, less constrained amorphous fraction and larger crystals, a more traditional elastomeric behavior. The permanent set is similar for the two samples, but $A_{25}$, characterized by smaller crystallites, more intimately connected with the amorphous and a larger intermediate phase component, shows both higher modulus and strain hardening. This features appear related to the limited extensibility of the chains forming the elastic network of $A_{25}$ and to its capacity to crystallize under stress.

## Introduction

In polymer technology the orientation of the crystalline and amorphous phases is highly relevant for the performance of polymeric materials in their applications. In turn, unidirectional cold drawing of polymeric films, performed to optimize their orientation, clearly shows that different initial structures can affect the final properties of the fibers.[1−3]

Attempts to rationalize the mechanical response of semicrystalline polymers in terms of their structure and morphology have been the subject of many studies[4−6] showing that the mechanical properties depend indeed on many factors, often hardly correlated, such as phase composition, features of the amorphous component, crystallite size and perfection, morphology, and polymorphism. These considerations are particularly relevant in the case of syndiotactic polypropylene (sPP), a polymer exhibiting highly variable mechanical properties, depending upon orientation, crystallinity, and polymorphism.[7−10] It is well-known that, when sPP is drawn and the tension released, the fibers undergo a large shrinkage becoming elastic. This elasticity, closely correlated to the structural organization of the oriented sample, is not shown at all by the original films. Difficulties correlating the elastic behavior to the structural organization of sPP are principally due to its complex polymorphism.

Four crystalline forms of sPP have been described so far. Forms I and II are characterized by chains in the $(T_2G_2)_n$ helical conformation,[11,12] whereas forms III and IV present chains in trans-planar and $(T_6G_2T_2G_2)_n$ conformations,[13,14] respectively. Form I is the stable form of sPP, obtained under the most common crystallization conditions either from the melt or from solution as single crystals.[11,15−18] Different kinds and amounts of disorder of the crystalline phase, depending on the degree of stereoregularity and the mechanical and thermal history, were described in rapidly crystallized samples.[18] In specimens quenched from the melt in a cold bath at 0 °C for many days, the presence of form III[19] or of a trans-planar mesophase[20] was recognized. Stretching either the helical form I or the trans-planar mesophase, the crystalline form III with the chains in trans-planar conformation is obtained when the sample is fixed at $\lambda$ around 6−7, whereas the starting conformations again form when the tension on the sample is relaxed.[9,10,21]

Many studies have been already presented, trying to understand the origin of the peculiar elastic behavior in sPP. Loos et al.[22] analyzing melt-spun sPP single filament fibers associated elasticity to low crystallinity and small micelle-like crystals in the fiber, acting as

* Corresponding author: e-mail vvittoria@unisa.it.

10.1021/ma040039e CCC: $27.50 
Published on Web 00/00/0000 PAGE EST: 7.7

physical cross-links in the amorphous matrix. Guadagno et al.[8−10,21] drawing at room temperature samples either in the helical or in the trans-planar form found that, despite the different, often complex, structural organization of the elastic fibers, their behavior was qualitatively very similar. Elasticity was proposed to be closely associated with—even though not necessarily dependent on—a helical/trans-planar conformational transition involving specifically tie molecules connecting different crystalline blocks and more in general the substantial amorphous fraction present in the samples. This result was confirmed studying a structurally simple fiber also showing elastic behavior, but in which the molecules in all ordered phases remained in the trans-planar conformation throughout the elongation and relaxation processes.[10] Auriemma et al.[23] analyzing fibers cold drawn at room temperature concluded that, in the case of sPP, the elastic behavior is basically linked to the enthalpy gain achieved when the sample is relaxed, which involves a crystal−crystal phase transition from the metastable form III to the more stable helical modification (form II).

In the present paper we report investigations concerning the structure and the elastic behavior of fibers obtained drawing samples crystallized in the helical form at two different temperatures. Along with the presence of the trans-planar mesophase in the original sample, the phase composition, the crystal dimensions were studied. The aim was to correlate these features with the final structure and properties of the resulting fibers in order to further clarify the problem of the unusual elasticity of syndiotactic polypropylene.

## Experimental Section

Syndiotactic polypropylene was synthesized according to established procedures.[7] The polymer was analyzed by $^{13}C$ NMR spectroscopy at 120 °C on a Bruker AM 250 spectrometer operating in the FT mode at 62.89 MHz by dissolving 30 mg of sample in 0.5 mL of $C_2D_2Cl_4$. Hexamethyldisiloxane was used as internal chemical shift reference. Our sample showed 91% syndiotactic pentads.

The sPP powders were molded in a hot press, at 150 °C, forming a 0.2 mm thick film, which was rapidly quenched in a bath at room temperature (sample $A_{25}$). A different film was quenched to 100 °C and left for 1 h at this temperature (sample $B_{100}$).

The two films were drawn at room temperature using an INSTRON 4301 dynamometric apparatus. The deformation rate was 10 mm/min, and the initial length of the sample was 10 mm. Two fibers were obtained drawing to $\lambda = 7$ and analyzed at fixed length (samples $A_{25}7$ and $B_{100}7$). The samples were subsequently released and a strong shrinkage to $\lambda = 4$ was observed (samples $A_{25}4$ and $B_{100}4$).

Wide-angle X-ray patterns (WAXD) were obtained using a Philips PW 1710 powder diffractometer (Ni-filtered Cu Kα radiation) with a scan rate of 2°($\theta$)/min.

Fiber diffraction spectra were recorded under vacuum by means of a cylindrical camera with radius of 57.3 mm and the X-ray beam perpendicular to the fiber axis (Ni-filtered Cu Kα radiation).

The transport properties were measured by a microgravimetric method, using a quartz spring balance having an extension of 20 mm/mg. The penetrant used was dichloromethane, and the experiments were carried out at 25 °C. Sorption was measured as a function of vapor activity, $a = p/p_0$, where $p$ is the actual pressure to which the sample was exposed and $p_0$ is the saturated vapor pressure at the temperature of the experiment.

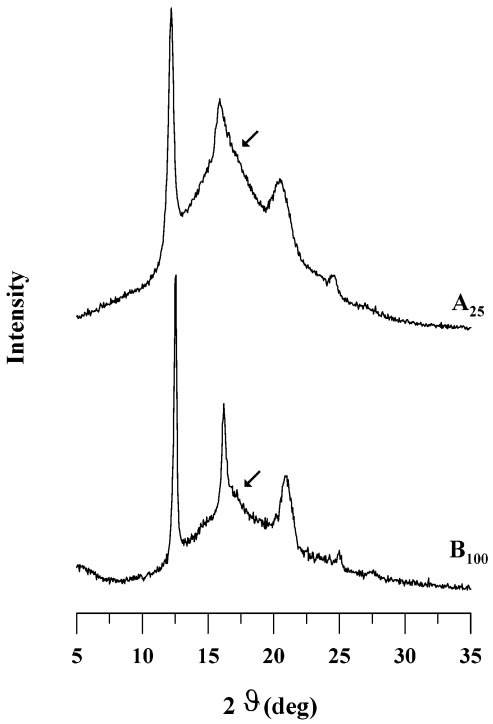


**Figure 1.** X-ray diffractograms of $A_{25}$ and $B_{100}$ samples.

## Results and Discussion

**Structure of the Initial Samples.** In Figure 1 we show the X-ray diffraction patterns of samples $A_{25}$ and $B_{100}$. Both indicate that the samples crystallized in the usual form I, characterized by the most intense peaks at 12.3°, corresponding to the 200 reflection, 15.9° corresponding to the 010 reflection, and 20.8° of $2\vartheta$, corresponding to the 210 reflection.

The absence of the 211 reflection at $2\vartheta = 18.9°$ indicates that we obtained in both samples the disordered modification of form I, as expected for samples crystallized at low temperatures: indeed, the preferential crystallization of the disordered form was always found in samples of low syndiotacticity or in powder samples crystallized from the melt at temperatures below 120 °C.[24] In this case, as well documented in other cases, departures from the fully antichiral packing both along *a* and *b* axes apparently occurs, leading to a less ordered form. Though characteristic of the same crystalline form, the two spectra show some evident differences: in particular, the profiles of sample $A_{25}$ are much broader and the peak at $2\vartheta = 15.9°$ is not symmetric, showing a shoulder at $2\vartheta = 17°$ (see arrow in Figure 1), typical of the trans-planar mesophase.[20] While it was previously shown that the trans-planar mesophase can be formed keeping the sample for a long time at 0 °C, and it is stable up to 60 °C,[20,25] the present result shows that it can be obtained, although as a minor component, also at 25 °C.

The diffraction patterns in Figure 1 indicate that qualitatively the amorphous contribution is larger in sample $A_{25}$ than in $B_{100}$. Using the pattern of atactic polypropylene to quantify the noncrystalline component, we derived an approximate crystallinity value for the two samples by comparing the area of the crystalline peaks with the total area, that is, $\alpha_c = A_c/(A_c + A_a)$, as reported in the literature.[26] The crystallinity is probably somewhat overestimated in this procedure, since the mesophase scattering will contribute, as it should, to

**Table 1. Crystallinity, $\alpha_c$, Crystallite Coherence Lengths Perpendicular to Reflection Planes 200 ($D_{200}$) and 010 ($D_{010}$), and Width at Half-Maximum, fwhm, Derived from X-ray Diffraction Measurements; the Fraction of Amorphous Phase, $\alpha_a$, the Fraction of Impermeable Phase, $\alpha_{imp} = 1 - \alpha_a$, and the Mesophase Fraction, $\alpha_m = \alpha_{imp} - \alpha_c$, Were Derived by Sorption at 0.2 Activity (Estimated Error Bars Are Supplied)**

| sample | $\alpha_c$ (%) | $\alpha_a$ (%) | $\alpha_{imp}$ (%) | $\alpha_m$ (%) | fwhm$_{200}$ ($2\vartheta$°) | $D_{200}$ (Å) | fwhm$_{010}$ ($2\vartheta$°) | $D_{010}$ (Å) |
|---|---|---|---|---|---|---|---|---|
| $A_{25}$ | 21 ± 2 | 52 ± 3 | 48 ± 2 | 27 ± 2 | 0.521 ± 0.020 | 307 ± 11 | 0.830 ± 0.022 | 193 ± 6 |
| $B_{100}$ | 30 ± 2 | 59 ± 3 | 41 ± 2 | 11 ± 2 | 0.274 ± 0.012 | 584 ± 25 | 0.371 ± 0.012 | 433 ± 13 |

the noncrystalline profile but also in some degree to the crystalline peaks. The crystallinity of sample $B_{100}$ is 30%, substantially higher than that of sample $A_{25}$ ($\alpha_c = 21\%$). Moreover, the profile sharpness of sample $B_{100}$ qualitatively indicates much larger crystals than in $A_{25}$. Quantitative results, using the Scherrer equation,[27] are also reported in Table 1 for the values of $D_{200}$, the coherent crystalline domain size in the direction perpendicular to the (200) planes, and of $D_{010}$, perpendicular to the (010) planes, obtained respectively from the full width at half-height (fwhm) of the 200 and 010 profiles. As expected, the values found for the crystallite dimensions are substantially smaller in the case of sample $A_{25}$, crystallized at room temperature, than in $B_{100}$. Surprisingly high are, on the other hand, the absolute values of the crystallite size as compared to values usually reported for polymers crystallized at relatively high undercoolings. These features point to an unusual ability of lamellar crystals of sPP helical modifications to host defects without losing coherence, at least in certain crystallographic directions. The implications of these observations will have to be considered carefully.

**Phase Composition.** The presence, in sample $A_{25}$, of the shoulder at $2\vartheta = 17°$, typical of the trans-planar mesophase, prompted us to investigate the phase composition on the basis of the transport properties of vapors at low activity. Procedures to obtain phase composition information from transport data are based on the assumption that the specific sorption of the amorphous phase is the same in samples having different composition, provided a low vapor activity is used. The rigid regions, usually crystalline, are generally impermeable to the vapors at low activity ($a \leq 0.4$). At a given vapor activity, we can write

$$C_{eq} = C_{eq(\text{amorphous sample})}\alpha_a$$

$$\alpha_a = 1 - \alpha_{imp}$$

where $C_{eq}$ is the equilibrium concentration of vapor in the sample at a given activity, $\alpha_a$ and $\alpha_{imp}$ are the fractions of the permeable (amorphous) and impermeable phase, respectively, and $C_{eq(\text{amorphous sample})}$ is the equilibrium concentration of a completely amorphous sample. If the sample only contains the amorphous and the crystalline phases, its sorption at low activity, compared to the sorption of a completely amorphous sample, gives the crystallinity $\alpha_c$ and the amorphous phase fraction $\alpha_a$. On the other hand, if the sample contains a mesophase, also impermeable to the vapors at low activity, the fraction $\alpha_{imp}$ of impermeable phase will correspond to the sum of the mesophase and the crystalline phase contributions. As a matter of fact, generally also mesophases are impermeable to the vapors at low activity.[28,29] As for the sorption of the amorphous sample, in our case, because it is not possible to obtain syndiotactic polypropylene in the amorphous state at room temperature, we refer to the sorption at low activity of atactic polypropylene. This assumption was found valid in the case of isotactic polypropylene at different crystallinities.[30]

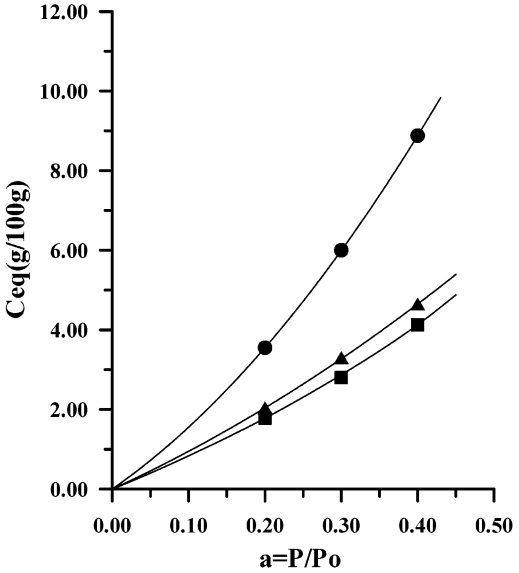


**Figure 2.** Equilibrium concentration of vapor as a function of vapor activity, $a = p/p_0$, for atactic polypropylene (●), sample $A_{25}$ (■), and sample $B_{100}$ (▲).

In Figure 2 the equilibrium concentration $C_{eq}$ (grams of vapor per 100 g of dry polymer) is reported for atactic polypropylene and for samples $A_{25}$ and $B_{100}$. At activity $a = 0.2$, we determined the amorphous fraction, $\alpha_a$, dividing the sorption of each sample by the sorption of atactic polypropylene. We obtained thus the fraction of impermeable phase $\alpha_{imp} = 1 - \alpha_a$, which is reported in Table 1 along with the crystallinity, derived from X-ray diffraction for the two samples. For both specimens the fraction of impermeable phase is significantly higher than the crystallinity. We were therefore able to evaluate the mesophase fraction in the two samples as the difference between the impermeable phase fraction and the X-ray crystallinity. The reliability of the vapor sorption method has been previously demonstrated for various polymeric systems: indeed, it has been always found that when no mesophase is present, it gives crystallinity values closely comparable to those obtained by X-ray diffraction (differences typically ≤3%).[28−34]

It may appear surprising that also sample $B_{100}$, crystallized at 100 °C, contains a small fraction of impermeable noncrystalline phase, but it probably formed when the sample was brought to room temperature, after isothermal crystallization. This finding is consistent with indications in the diffraction pattern of $B_{100}$ (see arrow in Figure 1), suggesting also in this sample a minor mesophase component, evidenced by the shoulder at $2\vartheta = 17°$. With the aim of eliminating this component, we also crystallized some samples at 100 °C for longer times (3 h) and annealed others at higher temperatures (at 120 °C for 3 h or at 130 °C for 1 h). Since in all these samples X-ray diffraction and the transport properties still indicated the presence of a

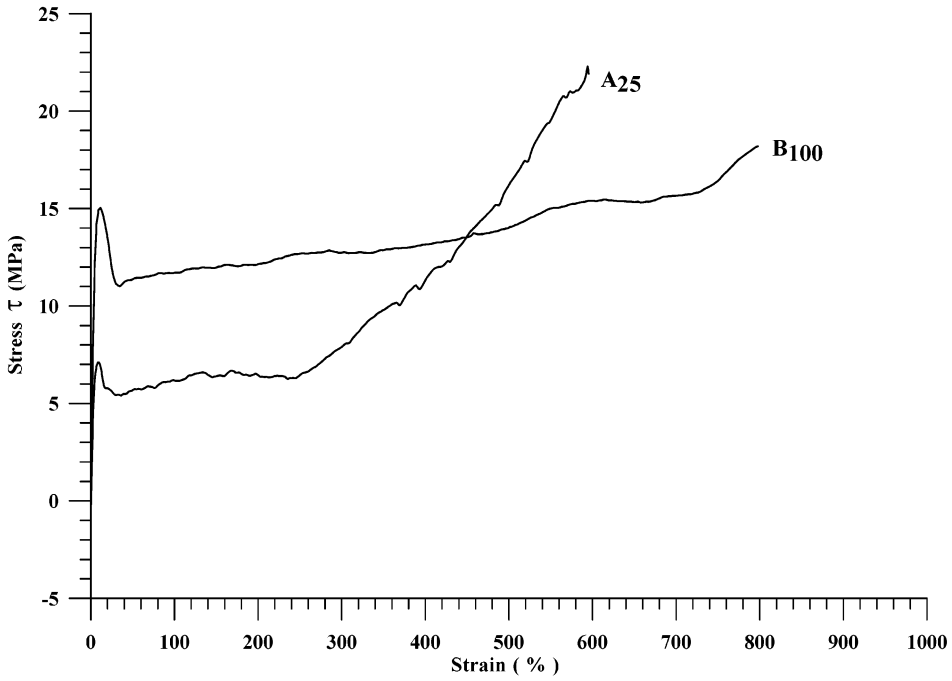


**Figure 3.** Stress−strain curves of $A_{25}$ and $B_{100}$ samples.

nonnegligible amount of mesophase, we concentrated on the $B_{100}$ sample, obtained with a simpler procedure.

**Drawing Behavior.** In Figure 3 we report the stress−strain curves obtained stretching, at room temperature, samples $A_{25}$ and $B_{100}$. The tensile stress on the initial undeformed cross-sectional area, $\tau$ (MPa), is reported as a function of the percentage of strain.

Both curves are conventional with an upper and lower yield point, restricted in a very narrow deformation range that, at a macroscopic level, characterizes the appearance of a neck. The local deformation drastically increases in the neck, producing a significant reduction in the local cross section. This effect, in turn, induces a stress concentration that stabilizes the neck, which propagates over all the sample. This stage of the drawing process occurs at an almost constant load, and only when the neck has propagated to the whole sample the stress begins increasing more rapidly up to fracture. We note that most of the amorphous orientation generally occurs in the strain-hardening range.

The two curves in Figure 3 are qualitatively similar, and we will try to relate the evident differences to the different structural organization of the two samples, in terms of crystallinity, crystal dimensions, and fraction of mesophase. Sample $B_{100}$ shows a much higher yield stress (15.0 MPa) and postyield stress drop (4.0 MPa) than sample $A_{25}$ (7.2 and 1.8 MPa, respectively). This is readily explained by the higher crystallinity and higher crystal dimensions, which are routinely related to the yield stress and the postyield stress drop. Moreover, observing the drawing curves, sample $A_{25}$ shows a well-defined deformation range in which stress increases very slowly: it is located between 20% and 250%, while beyond that point a substantial strain hardening is evident, extending up to fracture which occurs at 600% deformation. The curve of sample $B_{100}$ shows a very wide region between 20% and ca. 750% in which stress increases steadily but very slightly. Only in the very small range from 750% to the breaking point at ca. 800%, a higher increase of stress is observable. This different behavior determines an inversion of the curves: in fact, beyond 460% of deformation, sample $A_{25}$ shows a higher stress than sample $B_{100}$ and breaks at a lower deformation and a higher stress. Also, this behavior can be related to the structural differences between the two samples. Sample $B_{100}$ contains larger crystals, a more relaxed amorphous phase, and a lower fraction of mesophase. It is therefore less likely for the crystals to be connected by the intermediate phase, and we expect less entanglements in the amorphous phase, which indeed is more easily oriented, as shown by X-ray diffraction (see Figure 4). Instead, sample $A_{25}$ is characterized by crystals of smaller dimensions, connected by a component that does not behave as an amorphous phase, making the whole structure more rigid. Crystalline and amorphous phases in $A_{25}$ are tightly interconnected and respond to stress as a single system, more rigid than in the case of $B_{100}$. Sample $A_{25}$ can be oriented more easily at the beginning, but soon the connecting chains become extended and rapidly increasing stress is needed to further extend the sample. This high stress determines the fracture of the sample, which fails at a lower degree of orientation than $B_{100}$.

**Structure of the Fibers.** As reported in the Experimental Section, the fibers drawn up to $\lambda = 7$ undergo a large shrinkage on releasing the tension. The crystalline phase composition was investigated in both the fixed ($\lambda = 7$) and relaxed ($\lambda = 4$) fibers.

In Figure 4 we show the X-ray diffraction patterns of the fibers before ($A_{25}7$ and $B_{100}7$) and after releasing the tension ($A_{25}4$ and $B_{100}4$). Repeated cycles (three times) of stretching and releasing the fibers from $\lambda =$ 4.0 to $\lambda = 7.0$ demonstrate that the shown diffraction patterns are completly reproducible.

**Oriented Sample $A_{25}$.** In the pattern of the fixed sample $A_{25}7$ we observe, on the equator, the 020 ($2\theta =$ 15.9°), 110 ($2\theta = 18.8°$), and 130 ($2\theta = 29.5°$) reflections of the crystalline form III described by Chatani.[13] On the first layer, with a fiber repeat of 5.05 Å, the 021 ($2\theta = 23.7°$) and the very weak 111 ($2\theta = 25.8°$) reflections of the same modification are observable. Examining this pattern, we also note the presence of

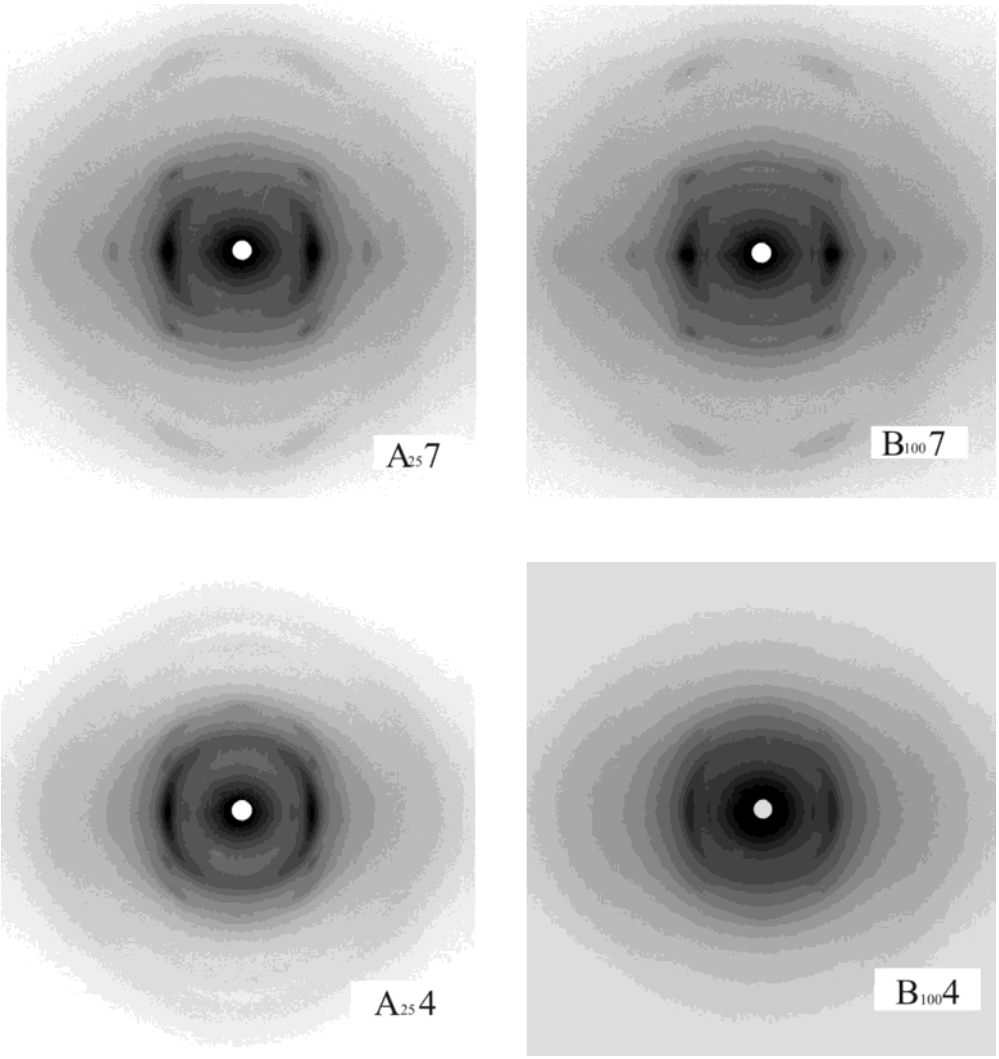


**Figure 4.** X-ray diffraction patterns of fibers before ($A_{25}7$ and $B_{100}7$) and after releasing the tension ($A_{25}4$ and $B_{100}4$).

some percentage of the trans-planar mesophase. In fact, the equatorial 020 and 110 reflections partially overlap with the reflection at $2\theta = 17.0°$, which, if associated with a reflection at $2\theta = 23.7°$ on the layer with periodicity 5.05 Å, has already been ascribed to a trans-planar mesophase adopting an orthohexagonal lattice[10] with $a = 6.02$, $b = 10.42$, and $c = 5.05$ Å. Therefore, in the $A_{25}7$ fiber the ordered phases are mainly the crystalline form III and the trans-planar mesophase. In the diffraction pattern of $A_{25}7$ we can however also observe, although hardly in the reproductions in Figure 4, a very weak reflection on the equator at $2\theta = 12.3°$ and a second one on the layer with 7.45 Å helical periodicity at $2\theta = 20.8°$, indicating that also traces of the helical modifications are present.

The pattern of the relaxed $A_{25}4$ fiber shows two intense reflections: a very strong one at $2\theta = 17.0°$ on the equator and a medium strong one at $2\theta = 23.7°$ on the layer characterized by a 5.05 Å periodicity. Both these reflections are typical of the trans-planar mesophase. Moreover in the $A_{25}4$ sample, highly polarized, medium-strong reflections, both on the equator ($2\theta = 12.3°$) and on the layer with periodicity 7.45 Å ($2\theta = 20.8°$), characteristic of the helical form, are apparent. Careful examination of Figure 4 suggests that in the pattern of $A_{25}4$ the amorphous halo around $2\theta = 17-18°$ appears to be more isotropic than in the $A_{25}7$ pattern. In the case of the $A_{25}4$ fiber the ordered phases are a mixture of a substantial amount of trans-planar mesophase and a small fraction of oriented crystalline helical form. The above data appear to indicate that form III, which is stable only under tension, upon relaxation, transforms essentially into the oriented trans-planar mesophase, as already found for fibers with a much simpler structural organization.[10] The present data do not allow to rule out the possibility that a fraction of the form III present in $A_{25}7$ transforms directly into crystals of the helical forms in $A_{25}4$. It is however more likely that, as we shall discuss more in depth in the conclusive remarks, the intensity increase of the helical reflections in the pattern of the $A_{25}4$ sample arises because some of oriented trans-planar mesophase, upon relaxing, transforms into the oriented helical forms. Similar results were already reported for sPP fibers prepared with different experimental procedures.[9,21]

**Oriented Sample $B_{100}$.** The discussed pattern of $A_{25}7$ is very different from that of $B_{100}7$, which shows two well-developed crystalline phases: form III and a helical form. We can observe that the equatorial reflections 020 and 110 of the crystalline form III are highly polarized and clearly separated. This implies a modest intensity at $2\theta = 17.0°$, denoting a minor fraction of trans-planar mesophase and a better developed form III with respect to sample $A_{25}7$. These observations are confirmed by the intensity of the layer reflections, namely the 021 reflec-

**Scheme 1. Structural Transformation Observed in the Two Samples $A_{25}$ and $B_{100}$**

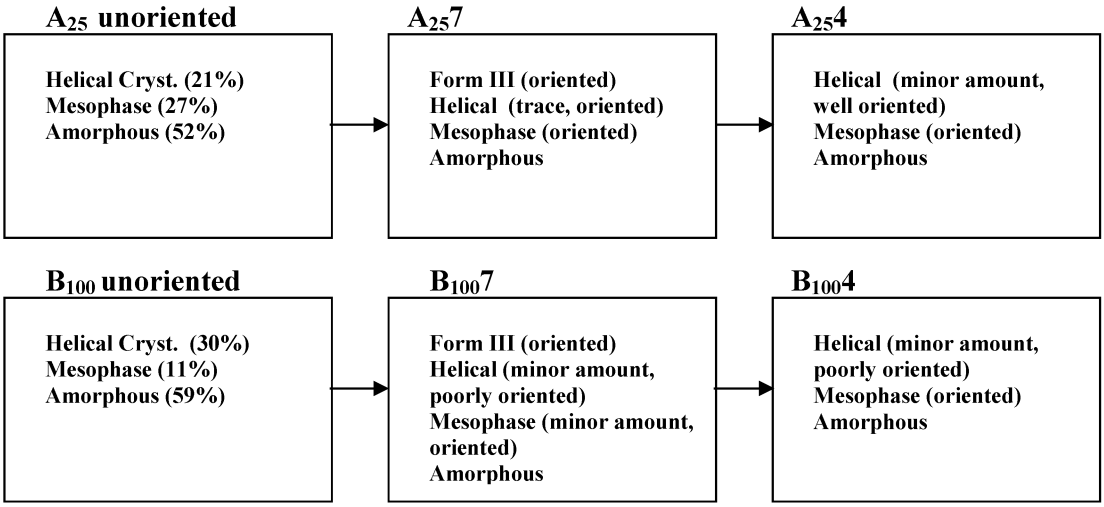


**Table 2. Mechanical Parameters of $A_{25}4$ and $B_{100}4$ Fibers: Elastic Modulus, Dissipated Energy, and Permanent Set**

| sample | elastic modulus (MPa) | dissipated energy (MPa) | | | set (%) | | |
|---|---|---|---|---|---|---|---|
| | | primary cycle | secondary cycle | tertiary cycle | primary cycle | secondary cycle | tertiary cycle |
| $A_{25}4$ | 178 | 117 | 375 | 804 | 8 | 19 | 28 |
| $B_{100}4$ | 100 | 61 | 209 | 388 | 6 | 16 | 27 |

tion, and the clear 111 reflection of form III. The second important feature in the $B_{100}7$ fiber is the presence of the crystallites of the helical forms very modestly oriented as compared to the trans-planar crystalline form III. In fact, the equatorial reflection at $2\theta = 12.3°$ has a large azimuthal spread, and the helical reflection at $2\theta = 20.8°$ appears as an almost isotropic ring.

Examination of the relaxed $B_{100}4$ fiber does not evidence any form III which was present in high proportion in the fully elongated $B_{100}7$ sample. We must conclude that, upon relaxing, form III transformed either completely or to a large extent, into the trans-planar mesophase, having a very intense peak at $2\theta = 17°$. As for the helical reflections their intensity is in essence unchanged, or possibly slightly increased, as compared to patterns of the fixed sample. The orientation is also practically unvaried with respect to $B_{100}7$ fiber. If there is a minor increase of the fraction of helical modifications, it may result, as discussed for fiber $A_{25}$, either from form III crystals of the helical forms transition or, more plausibly, via the mesophase. To a first approximation we can state that both stretching and relaxing fiber $B_{100}7$ in the elastic range (i.e., between $\lambda = 4$ and $\lambda = 7$), crystals of the helical forms do not undergo any significant change. This fact implies that the observed elastic behavior is largely independent of structural changes within crystals of the helical modifications, which in the present case act as a rigid component embedded in a softer, deformable matrix consisting of the amorphous phase and of trans-planar mesophase domains. At variance, the mesophase domains are converted into the crystalline form III by the applied stress through a mechanism of largely reversible and cooperative chain movements. This speculative but plausible conclusion follows from the structural similarity between the trans-planar mesophase and form III, suggesting that the transitions between these two phases do not proceed by a melting−recrystallization process.

The structural transformations observed in the two samples $A_{25}$ and $B_{100}$ are reported in Scheme 1.

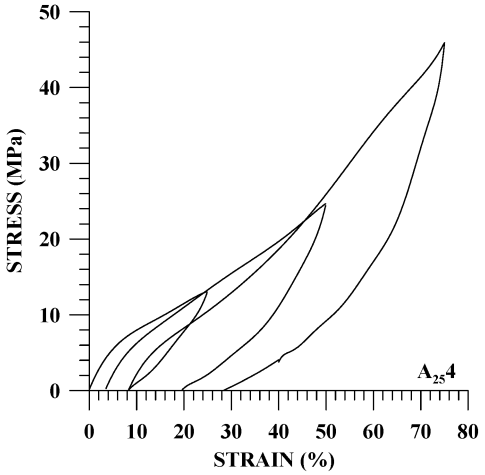


**Figure 5.** Hysteresis cycles of sample $A_{25}4$: first cycle strain (%) = 24, second cycle strain (%) = 49, and third cycle strain (%) = 73.

**Elastic Behavior.** The elastic modulus of the two fibers, measured at very low strain, is reported in Table 2. The value for sample $A_{25}4$ is almost double than for sample $B_{100}4$, consistent with the above-discussed drawing behavior. In the range between $\lambda = 4.0$ (relaxed fiber) and $\lambda = 7$ (fixed fiber), the two fibers show elastic behavior. In Figures 5 and 6 we report the hysteresis cycles of samples $A_{25}4$ and $B_{100}4$, which were deformed at strain values progressively increasing, step by step, from the relaxed length ($\lambda = 4.0$) to the highest previously reached length ($\lambda = 7$), recording the stress while increasing and decreasing the strain. The highest previously reached length was not exceeded to reduce the possibility of additional plastic deformation of the fibers during the measurement of the elastic recovery. The area of each hysteresis curve, reported in Table 2, represents the energy dissipated in the cycle and increases on increasing the strain. The permanent set, that is, the residual deformation after each cycle, also reported in Table 2, is low for both samples, reaching values of 27% and 28% for the maximum strain, and it

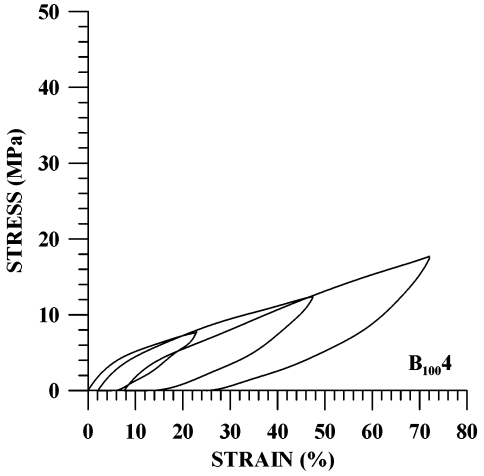


**Figure 6.** Hysteresis cycles of sample $B_{100}4$: first cycle strain (%) = 24, second cycle strain (%) = 49, and third cycle strain (%) = 73.

nearly vanishes after 2 h at rest. Although the elastic behavior of the two fibers is very similar, some relevant differences are observable. Specifically, the areas of the hysteresis curves of sample $A_{25}4$ are much higher than those of sample $B_{100}4$, and substantial strain hardening in the third cycle is observable for $A_{25}4$ but not for $B_{100}4$. The stress in the case of sample $A_{25}4$ reaches 46 MPa at $\lambda = 7$ to be compared with 16 MPa for sample $B_{100}4$ at the same elongation. Also in this respect we can ascribe the differences to the morphological organization resulting from drawing different initial structures. In fiber $A_{25}4$ the amorphous phase and the crystalline phase are more intimately connected, and this in turn determines a higher modulus and a higher capacity to crystallize under stress, evidenced by the intense strain hardening. In fiber $B_{100}4$ the amorphous phase is more relaxed, and it behaves as a conventional elastomer, hardly showing any strain hardening.

To better investigate the differences, the stress−strain data of the third cycle for sample $A_{25}4$ and $B_{100}4$ were evaluated in terms of the Mooney−Rivlin equation[35]

$$\tau = 2C_1(\lambda - \lambda^{-2}) + 2C_2(\lambda - \lambda^{-2})\frac{1}{\lambda}$$

where $\tau$ is the force per unit of cross-sectional area, $\lambda$ is the strain ratio, and $C_1$ and $C_2$ are two numerical coefficients. In Figure 7 we show $\tau/(\lambda - \lambda^{-2})$ as a function of $1/\lambda$ for $A_{25}4$ and $B_{100}4$ fibers. A conventional behavior is observed for sample $B_{100}4$, for which the stress is linearly dependent on $1/\lambda$. At variance a strong upturn in the Mooney−Rivlin plot is observable for sample $A_{25}4$. This upturn is characterized by a rapid change of the $C_2$ term from positive to negative values. Indeed, this feature emphasizes the difference in the elastic behavior between the two samples and represents additional evidence of the different structural organization of the amorphous component in sPP fibers obtained from different initial structures.

In the literature the molecular origin of the upturn in the Mooney−Rivlin representation has been the source of considerable controversy. It has been attributed either to the *limited extensibility* of the chains in the elastic network, that is, to a non-Gaussian behavior, or to strain-induced crystallization. Either explanation is in principle compatible with the presence

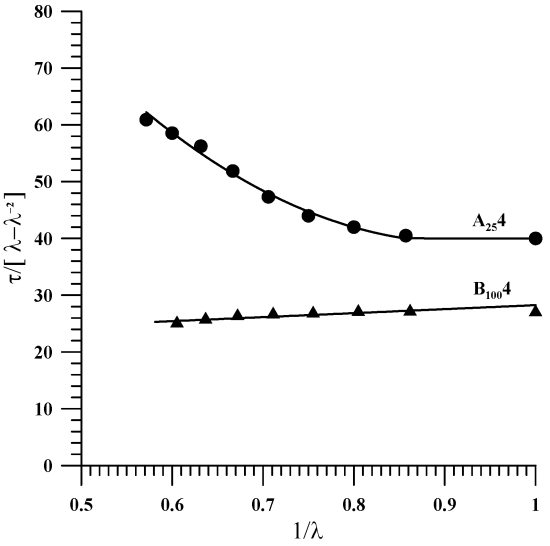


**Figure 7.** Ratio $\tau/[\lambda - \lambda^{-2}]$ as a function of $1/\lambda$ for $A_{25}4$ and $B_{100}4$ samples.

of the upturn in the Mooney−Rivlin plot of sample $A_{25}$. The presented experimental results indicate that the amorphous fraction, the crystallinity, and the crystallite size are all substantially smaller in the $A_{25}$ sample as compared to $B_{100}$. In $A_{25}$ the trans-planar mesophase is a more substantial component and constrains the amorphous chains which are less extensible. At variance sample $B_{100}$ with a more relaxed and less connected amorphous phase shows a conventional elastic plot. The phase composition analysis shows that both samples present strain-induced crystallization of the mesophase into form III: such a process is in essence complete in the case of sample $B_{100}7$ while in $A_{25}7$ a substantial amount of mesomorphic phase remains. These observations indicate that the difference in mechanical properties between the two samples are more likely to relate to a tighter elastic network in the case of $A_{25}$ since strain-induced crystallization is more complete in $B_{100}7$. Work is in progress to investigate more in detail the morphology of the stretched samples and, in light of the present results, the elastic response of different morphologies.

## Concluding Remarks

The results of the present study evidence the effect of the crystallization temperature on the morphology of two sPP samples, in terms of crystallinity, crystal dimensions, and fraction of trans-planar mesophase. The two specimens $A_{25}$ and $B_{100}$, crystallized respectively at 25 and 100 °C, when drawn at room temperature to $\lambda = 7$, show a large shrinkage upon releasing the tension, reaching $\lambda = 4$. In the interval between the extended and the contracted state, the fibers show elastic behavior. The drawing behavior of both sPP specimen is clearly influenced by the initial morphology. Mechanical parameters, like the elastic modulus, the elongation at break, etc., appear to correlate qualitatively with the phase composition, the crystallite size, and their orientation.

The fixed $B_{100}7$ and $A_{25}7$ fibers ($\lambda = 7$) are characterized by the presence of large amounts of the crystalline form III. However, in the case of the fiber $B_{100}7$, obtained from the $B_{100}$ film with larger crystals of the helical forms, the remaining fraction of mesophase is clearly smaller than in the $A_{25}7$ fiber. As discussed in a

previous work,[10] the mesophase present in the unoriented samples largely transforms into form III. The transformation would be complete if values of $\lambda$ greater than 9 could be imposed. We had to limit the draw ratio to 7 because sample $A_{25}$ breaks at larger values. On the other hand, in the stretching process some mesophase can develop from crystals of the helical forms and from the amorphous phase. In $B_{100}7$ a fraction of crystals of the helical form scarcely oriented are evidenced by the X-ray pattern. This fraction remains almost unchanged in the relaxed $B_{100}4$ fiber.

In the fiber derived from the $A_{25}$ film, with smaller crystals of the helical forms and a higher fraction of mesophase, the presence of crystals of the helical forms is almost negligible in the $A_{25}7$ extended fiber and remains low in the relaxed $A_{25}4$. Furthermore, a substantial amount of the trans-planar mesophase present in $A_{25}4$ is found also in $A_{25}7$, along with form III, which crystallizes upon stretching. The fact that the mesomorphic component does not fully crystallize, that lower elongations at break can be achieved, and that a higher modulus is observed all point to a highly stressed state of the mesophase in $A_{25}7$. Furthermore, crystals of the helical forms, and crystallization into these forms, appear to play a minor role in the elastic behavior of our samples. All these observations are in full agreement with recent results on sPP fibers which do not contain crystals of the helical modifications[10] but display the characteristic elastic behavior of this polymer.

Although a more quantitative morphological analysis of the fibers would be desirable, and related work is indeed in progress, it appears safe to conclude that the elastic behavior of the two investigated samples depends largely on the amorphous and the mesomorphic components: when the amorphous phase and the crystalline phase are more intimately connected by a stressed mesomorphic component, as in sample $A_{25}$, a higher modulus and a nonconventional elastic behavior are observed. At variance, when the amorphous and the mesomorphic phase are more relaxed as in $B_{100}$, the fiber behaves as a conventional elastomer: it shows very modest strain hardening effects and follows the Mooney–Rivlin equation.

**Acknowledgment.** We are pleased to acknowledge financial support by MIUR-Italia PRIN 2002, PRIN 2003, and "Liquid crystals and macromolecules for nano-organized structures".

## References and Notes

(1) de Candia, F.; Romano, G.; Russo, R.; Vittoria, V. *Colloid Polym. Sci.* **1987**, *265*, 696.
(2) Peterlin, A. *J. Polym. Sci.* **1965**, *C9*, 61.
(3) Peterlin, A. In *Ultra High Modulus Polymers*; Ciferri, A., Ward, I. W., Eds.; Applied Sciences: Barking. England, 1979.
(4) Bassett, D. C. *Principles of Polymer Morphology*; Cambridge University Press: Cambridge, 1981.
(5) Ward, J. M. *Mech. Prop. Solid Polym.*, in press.
(6) de Candia, F.; Russo, R.; Vittoria, V. *J. Appl. Polym. Sci.* **1987**, *34*, 698.
(7) Guadagno, L.; Fontanella, C.; Vittoria, V.; Longo, P. *J. Polym. Sci., Part C* **1999**, *37*, 173.
(8) D'Aniello, C.; Guadagno, L.; Naddeo, C.; Vittoria, V. *Macromol. Rapid Commun.* **2000**, *21*, 104.
(9) Guadagno, L.; D'Aniello, C.; Naddeo, C.; Vittoria, V. *Macromolecules* **2001**, *34*, 2512.
(10) Guadagno, L.; D'Aniello, C.; Naddeo, C.; Vittoria, V.; Meille, S. V. *Macromolecules* **2002**, *35*, 3921.
(11) Lotz, B.; Lovinger, A. J.; Cais, R. E. *Macromolecules* **1988**, *21*, 2375.
(12) De Rosa, C.; Corradini, P. *Macromolecules* **1993**, *26*, 5711.
(13) Chatani, Y.; Maruyama, H.; Noguchi, K.; Asanuma, T.; Shiomura, T. *J. Polym. Sci., Part C* **1990**, *28*, 393.
(14) Chatani, Y.; Maruyama, H.; Asanuma, T.; Shiomura, T. J. *J. Polym. Sci., Polym. Phys. Ed.* **1991**, *29*, 1649.
(15) Lovinger, A. J.; Lotz, B.; Cais, R. E. *Polymer* **1990**, *31*, 2253.
(16) Lovinger, A. J.; Davis, D. D.; Lotz, B. *Macromolecules* **1991**, *24*, 552.
(17) Lovinger, A. J.; Lotz, B.; Davis, D. D.; Padden, F. J. *Macromolecules* **1993**, *26*, 3494.
(18) De Rosa, C.; Auriemma, F.; Vinti, V. *Macromolecules* **1997**, *30*, 4137.
(19) Nakaoki, T.; Ohira, Y.; Hayashi, H. *Macromolecules* **1998**, *31*, 2705.
(20) Vittoria, V.; Guadagno, L.; Comotti, A.; Simonutti, R.; Auriemma, F.; De Rosa, C. *Macromolecules* **2000**, *33*, 6200.
(21) **)** Guadagno, L.; D'Aniello, C.; Naddeo, C.; Vittoria, V. *Macromolecules* **2000**, *33*, 6023.
(22) Loos, J.; Shimanski, T. *Polym. Eng. Sci.* **2000**, *40*, 567.
(23) Auriemma, F.; Ruiz de Ballestreros, O.; De Rosa, C. *Macromolecules* **2001**, *34*, 4485.
(24) De Rosa, C.; Corradini, P. *Macromolecules* **1993**, *26*, 5719.
(25) Guadagno, L.; D'Aniello, C.; Naddeo, C.; Vittoria, V.; Meille, S. *Macromolecules* **2003**, *36*, 6756.
(26) Natta, G.; Corradini, P.; Cesari, M. R. *Acc. Lincei* **1957**, *s 8*, 22, 11.
(27) Tadokoro, H. *Structure of Crystalline Polymers;* John Wiley; New York.
(28) Vittoria, V.; Perullo, A. *J. Polym. Sci., Part B: Polym. Phys.* **1986**, *25*, 267.
(29) Guadagno, L.; D'Arienzo, L.; Vittoria, V.; Longo, P.; Romano, G. *J. Macromol. Sci., Phys.* **2000**, *B39*, 425.
(30) Vittoria, V. *J. Polym. Sci., Polym. Phys.* **1986**, *24*, 241.
(31) Vittoria, V. *J. Macromol. Sci., Phys.* **1989**, *B28*, 97.
(32) Vittoria, V. *J. Macromol. Sci., Phys. Ed.* **1989**, *B28*, 489.
(33) Michele, A.; Vittoria, V. *Polym. Commun.* **1991**, *32*, 232.
(34) Vittoria, V. *J. Mater. Sci.* **1995**, *30*, 3954.
(35) Treolar, L. R. G. *The Physics of Rubber Elasticity*, 2nd ed.; Oxford University Press: New York, 1958.

MA040039E